Atmos. Chem. Phys. Discuss., 14, 29459–29497, 2014
www.atmos-chem-phys-discuss.net/14/29459/2014/
doi:10.5194/acpd-14-29459-2014

Atmospheric Chemistry and Physics Discussions
Open Access

Simulation of the isotopic composition of stratospheric water vapour – Part 2: Investigation of HDO/H_2O variations

R. Eichinger[1], P. Jöckel[1], and S. Lossow[2]

[1]Deutsches Zentrum für Luft- und Raumfahrt e.V. (DLR), Institut für Physik der Atmosphäre, Münchner Straße 20, Oberpfaffenhofen, 82234 Weßling, Germany
[2]Karlsruhe Institute of Technology, Institute for Meteorology and Climate Research, Hermann-von Helmholtz-Platz 1, 76344 Leopoldshafen, Germany

Received: 22 September 2014 – Accepted: 30 October 2014 – Published: 27 November 2014

Correspondence to: R. Eichinger (roland.eichinger@dlr.de)

Published by Copernicus Publications on behalf of the European Geosciences Union.

Abstract

Studying the isotopic composition of water vapour in the lower stratosphere can reveal the driving mechanisms of changes in the stratospheric water vapour budget and therefore help to explain the trends and variations of stratospheric water vapour during the recent decades. We equipped a global chemistry climate model with a description of the water isotopologue HDO, comprising its physical and chemical fractionation effects throughout the hydrological cycle. We use this model to improve our understanding of the processes, which determine the patterns in the stratospheric water isotope composition and in the water vapour budget, itself. The link between the water vapour budget and its isotopic composition in the tropical stratosphere is presented through their correlation in a simulated 21 year time series. The two quantities depend on the same processes, however, are influenced with different strengths. A sensitivity experiment shows that fractionation effects during the oxidation of methane has a damping effect on the stratospheric tape recorder signal in the water isotope ratio. Moreover, the chemically produced high water isotope ratios overshadow the tape recorder in the upper stratosphere. Investigating the origin of the boreal summer tape recorder signal in the lower stratosphere reveals isotopically enriched water vapour crossing the tropopause over the subtropical Western Pacific. A correlation analysis confirms this link, which identifies the Asian Summer Monsoon as the major contributor for the intrusion of isotopically enriched water vapour into the stratosphere during boreal summer. Furthermore, convective ice lofting is shown to have a substantial impact on the isotope ratios of water vapour in the upper troposphere and lower stratosphere.

1 Introduction

Variations of stratospheric water vapour alter the radiative heat budget (Forster and Shine, 1999) and the ozone mixing ratios (Shindell, 2001). The processes which control the stratospheric water vapour budget, however, are poorly quantified (Fueglistaler

ACPD
14, 29459–29497, 2014

et al., 2009). These processes are temperature-controlled dehydration, convective activity methane oxidation and isentropic transport.

Due to their physical and chemical properties, water isotopologues have the potential to answer the open questions concerning the origin of stratospheric water vapour. The small mass difference between H_2O and HDO lead to different vapour pressures and zero-point energies, respectively. This causes equilibrium and kinetic fractionation effects during phase changes and chemical reactions. Each process which controls the stratospheric water vapour budget can be associated with certain fractionation effects and therefore leaves a specific isotopic signature in the water vapour compound (see Moyer et al., 1996; Steinwagner et al., 2010). This isotopic fingerprint allows to comprehend the history of stratospheric water vapour (Johnson et al., 2001) and therewith, can assist to explain the trends and variations of its budget.

In addition to in situ and remote sensing measurements, the comprehensive simulation of the physical and chemical processes of water isotopologues on the global scale is needed to gain an improved understanding of the basic structure of the water isotope ratios in the stratosphere. Model studies of water isotopologues in the upper troposphere lower stratosphere (UTLS) include approaches from conceptional (Dessler and Sherwood, 2003; Bolot et al., 2013), to one-dimensional (Ridal et al., 2001; Zahn et al., 2006) and two-dimensional (Ridal and Siskind, 2002) models. Schmidt et al. (2005) applied the general circulation model (GCM) GISS-E, in order to study stratospheric entry values of the isotope ratios of water vapour. However, this model has a comparatively low resolution in the stratosphere and the accounting for methane oxidation is prescribed with a fixed production rate.

In the companion article (Eichinger et al., 2014) an extension of the global climate chemistry model (CCM) EMAC (ECHAM MESSy Atmospheric Chemistry) (MESSy: Modular Earth Submodel System; Jöckel et al., 2010) was presented and evaluated. This extension, namely the H2OISO submodel, comprises a separate hydrological cycle, including the water isotopologues $H_2^{18}O$ and HDO and their physical fractionation effects, based on previous studies by e.g. Hoffmann et al. (1998) and Werner

ACPD
14, 29459–29497, 2014

et al. (2011). Besides using sufficient vertical resolution that the tropical tropopause layer (TTL) is well resolved and explicit stratospheric dynamics, this expanded model system also includes the computation of the methane isotopologue CH_3D and its chemical contribution to HDO through oxidation. Results of an EMAC simulation showed good agreement in stratospheric HDO and $\delta D(H_2O)$ ($\delta D(H_2O) = \frac{[HDO]/[H_2O]}{R_{VSMOW}}$; ($R_{VSMOW} = 155.76 \times 10^{-6}$; Hagemann et al., 1970); VSMOW: Vienna Standard Mean Ocean Water) with measurements from several satellite instruments. Moreover, they revealed a stratospheric tape recorder, which ranges between the pronounced signal of MIPAS (Michelson Interferometer for Passive Atmospheric Sounding) satellite observations (see Steinwagner et al., 2010) and the missing upward propagation of the seasonal signal in the ACE-FTS (Atmospheric Chemistry Experiment Fourier Transform Spectrometer) satellite retrieval (see Randel et al., 2012).

The results of this simulation are now further analysed, aiming to identify the processes, which determine the patterns of the isotopic signatures in stratospheric water vapour. The connection between the water vapour budget and its isotope ratio in the tropical stratosphere over the two simulated decades is presented in Sect. 3. The influence of isotope effects during methane oxidation on the $\delta D(H_2O)$ tape recorder signal is investigated in Sect. 4. In Sects. 5 and 6 the $\delta D(H_2O)$ tape recorder is traced back to its origin, by examining the contributions of different Monsoon Systems and convective ice lofting on the isotopic compsition of water vapour in the UTLS. These analyses also reveal a possible underestimation of ice overshooting in the applied convection scheme, which can have a significant effect on $\delta D(H_2O)$ in the lower stratosphere. This study constitutes the initiation of the application of the new process diagnostics provided by the isotopic composition of water vapour for exploring the reasons for changes in the stratospheric water vapour budget in global atmosphere chemistry-climate models.

ACPD
14, 29459–29497, 2014

2 Model description and simulation setup

The MESSy-conform H2OISO submodel in the framework of the EMAC model (Jöckel et al., 2005, 2010) comprises a separate hydrological cycle, including tracers (Jöckel et al., 2008) for the water isotopologues $H_2^{16}O$, HDO and $H_2^{18}O$, in the three phases (vapour, liquid and ice), respectively. These tracers are treated identically to the standard state variables for water in the regular hydrological cycle of EMAC, with the addition of the physical fractionation effects for the isotopologues during phase transitions. The representation of these effects follows water isotopologue-enabled ECHAM (**EC**MWF **Ham**burg) model versions (see Hoffmann et al., 1998; Werner et al., 2001, 2011). Supplementary, an explicit accounting for the contribution of CH_3D oxidation to HDO has been developed, in order to achieve realistic HDO mixing ratios and $\delta D(H_2O)$ values in the stratosphere. In the companion part 1 of this article (Eichinger et al., 2014), the model system and the implementation of HDO throughout the hydrological cycle, including its chemical representation is presented in detail.

An EMAC simulation in the T42L90MA ($\sim 2.8^{\circ}$, 90 layers in the vertical – up to 80 km (0.01 hPa), explicit middle atmospheric dynamics) resolution was carried out. The simulation was performed with specified dynamics (i.e., "nudged" towards ERA-Interim reanalysis data ECMWF; Dee et al., 2011). The "Tiedtke-Nordeng" convection scheme (Tiedtke, 1989; Nordeng, 1994) was applied for the simulation. After starting from steady-state initial conditions in 1982, the simulation was evaluated during the 21 years from 1990 to 2011. A detailed description of the simulation setup, a description of the applied MESSy submodels and an extensive evaluation of the simulation is given in part 1 of this article (Eichinger et al., 2014).

3 Time series of H_2O and $\delta D(H_2O)$

Temporal variations in stratospheric water vapour during the last decades have been observed consistently by various instruments. The reasons for these variations are

ACPD
14, 29459–29497, 2014

much discussed (see e.g. Hurst et al., 2011; Dessler et al., 2013; Randel and Jensen, 2013). Before analysing these changes with the EMAC model using the newly implemented HDO, it has to be assured that the EMAC simulation features the main characteristics of the changes in stratospheric water vapour from 1990 to 2011. Therefore, the equatorial water vapour mixing ratios at 30 km altitude of the simulation are compared with a combined HALOE (HALogen Occultation Experiment) and MIPAS data set in Fig. 1. A detailed description of the combination of the satellite data time series is given in the Supplement. A two year running mean was calculated for both time series in order to make the trends more visible by eliminating the signal of the Quasi-Biennial Oscillation (QBO).

The combined HALOE/MIPAS observations show an increase in stratospheric water vapour in the first half of the 1990s and a plateau hereafter until the year 2000. The water vapour mixing ratio drops by around 0.3 $\mu mol\,mol^{-1}$ between 2000 and 2002 and stays at this lower level until the middle of the first decade of the 21st century. Hereafter, a slow increase can be observed until the end of the time series in 2012. This behaviour of stratospheric water vapour during the previous decades has also been reported and discussed e.g., by Randel and Jensen (2013) analysing a combined HALOE and MLS (Microwave Limb Sounder) data set, and is strongly connected to tropopause temperatures.

The EMAC simulation generally reproduces these variations, although with a constant offset and a few differences. The drop around the year 2001 is preceded by an increase in water vapour. Moreover, in contrast to the satellite observations, the level of the water vapour mixing ratio after the drop does not fall below the level of the early 1990s.

In order to estimate the correlation between the changes of water vapour and its isotopic composition, the monthly anomalies (w.r.t. the 21 year monthly averages of the tropical water vapour mixing ratio and $\delta D(H_2O)$) are shown in Fig. 2 for the 21 years of the EMAC simulation at 18 km and at 30 km altitude, respectively. Again, the data

ACPD
14, 29459–29497, 2014

was processed with a two year running mean, in order to obtain a better visibility of the trends. The anomaly of $\delta D(H_2O)$ is scaled with 1/30 for better comparability.

At 18 km altitude, the Pearson's correlation (a description is given in the Supplement) between the two time series is 0.58 and this correlation decreases to 0.27 at 30 km. At 18 km altitude, the troposphere-stratosphere exchange processes are determining for both quantities. At 30 km altitude, the chemical effects induced by CH_4 oxidation for H_2O and the different life times of CH_4 and CH_3D for $\delta D(H_2O)$ are dominating. An interdependence of the two quantities can be observed at both altitudes, although, during certain periods, the development of the two time series is opposing. The drop around the year 2001 can be seen in water vapour and in $\delta D(H_2O)$ at both altitudes. At 18 km, the more pronounced feature in $\delta D(H_2O)$, however, is the steep increase before the drop. The amplitude of this increase in $\delta D(H_2O)$ exceeds the amplitude of the drop almost by a factor of 2. Even though most of the variations of the two quantities are oriented similarly, the sign of the anomalies is sometimes opposing. At 18 km altitude, $\delta D(H_2O)$ is generally at a lower level at the end of the 1990s compared to the early 2000s, after the drop. The short-term changes in particular seem to be different between the two quantities. This suggests, that the processes that control stratospheric $\delta D(H_2O)$ are related, but not equal to those that control the stratospheric water vapour budget. The tropopause temperatures, methane oxidation, convective activity or other processes determining water vapour in the stratosphere are thus affecting stratospheric H_2O and $\delta D(H_2O)$ with different strengths. Knowledge of this behaviour can therefore help to address the origin of certain variations and trends to changes in specific processes. The next sections are thus aiming on working out the influence of individual processes on stratospheric $\delta D(H_2O)$, with a special focus on the tape recorder, since the strength of this phenomenon determines the intrusion of water vapour into the stratosphere.

ACPD
14, 29459–29497, 2014

4 Sensitivity of the $\delta D(H_2O)$ tape recorder to methane oxidation

In order to analyse the impact of the contribution of CH_4 and CH_3D oxidation on the $\delta D(H_2O)$ tape recorder signal, an additional EMAC simulation was conducted. The only difference of this simulation is a modified chemical tendency for HDO. The concept for this sensitivity simulation is an artificial deactivation of the chemical fractionation effects. In other words, $\delta D(H_2O)$ does not get influenced by chemical isotope effects, CH_3D oxidation alters HDO always in relation to CH_4 oxidation, as if there was no isotope fractionation. A detailed description of this modification is given in the Supplement.

For the analysis of the impact of isotope effects during methane oxidation on the $\delta D(H_2O)$ tape recorder signal, the simulation with modified HDO tendency is compared to the simulation with regular methane isotope chemistry. The setup is the same for both simulations. Figures 3 and 4 show the tropical tape recorder signal from 2004 to 2009 for the two simulations from 15 to 30 km.

Between 15 and 20 km the $\delta D(H_2O)$ values are similar in both figures. In the tropical tropopause layer and the lower stratosphere, $\delta D(H_2O)$ is only weakly affected by methane oxidation. From 20 km upwards, increasingly higher $\delta D(H_2O)$ values can be observed in Fig. 3. The effect of the chemistry on $\delta D(H_2O)$ increases with altitude in the stratosphere. This can be observed for the increased $\delta D(H_2O)$ values, which emerge during NH summer, as well as for the low $\delta D(H_2O)$ values from the boreal winter signal. The tape recorder signal in Fig. 4 is stronger and reaches higher up. It is still present, although weak, at the top of the figure at around 30 km altitude. In Fig. 3 the $\delta D(H_2O)$ tape recorder signal above 25 km is entirely overshadowed by high $\delta D(H_2O)$ values, which are generated by the different life times of CH_4 and CH_3D. The upward propagating signatures fade out, or rather mix in with the high $\delta D(H_2O)$ values.

For a better quantification of the differences of the two tape recorder signals, Fig. 5 shows the averaged amplitudes of the $\delta D(H_2O)$ tape recorder signals with altitude. The black line denotes the simulation with, and the red line the simulation without the methane effect.

ACPD
14, 29459–29497, 2014

The tape recorder amplitudes are equal below the lower stratosphere. As expected, further above, the amplitude of the simulation with chemistry effect on $\delta D(H_2O)$ decreases faster with altitude than the amplitude of the simulation without this effect. The high $\delta D(H_2O)$ values from the NH summer signal are not affected as strongly by methane oxidation as the low values from the NH winter signal. To explain this, constant temperatures, and hence fractionation factors, and a constant background $\delta D(CH_4)$ are assumed, which is reasonable here. The isotope ratios of isotopically different reservoirs possess different sensitivities to the addition of a compound with a certain isotope ratio. This means that the smaller the differences between the δ values are, the smaller is the alteration. Since the high $\delta D(H_2O)$ values from the NH summer signal are closer to the $\delta D(CH_4)$ ($\delta D(CH_4)$ is also based on VSMOW) values, which are around −50 ‰ here (not shown), compared to the low $\delta D(H_2O)$ values from NH winter, the summer signal is altered less. Additionally, also the water vapour mixing ratios are different here. The δD values of the low water vapour mixing ratios from the NH winter signal are therefore again affected stronger by the addition of (a similar amount of) isotopically enriched water vapour from methane oxidation. This concludes that the production of H_2O and HDO by the oxidation of CH_4 and CH_3D, reduces the amplitude of the $\delta D(H_2O)$ tape recorder and overshadows the upward propagation of the signal.

Above 23 km, the amplitude of the $\delta D(H_2O)$ variations of the simulation with chemistry effect on $\delta D(H_2O)$ exceeds the amplitude of the simulation without. This, however, is not due to the tape recorder effect anymore. It is due to temperature and hence chemical fractionation factor variations caused by the QBO. The cycle of the QBO can be seen in the high $\delta D(H_2O)$ values between 25 and 30 km in Fig. 3. The QBO also has an effect on the stratospheric water vapour budget and on the water vapour tape recorder (see Niwano et al., 2003).

ACPD
14, 29459–29497, 2014

5 The origin of the $\delta D(H_2O)$ tape recorder

5.1 The pathway of isotopically enriched water vapour into the tropical stratosphere

In order to analyse the origin of the $\delta D(H_2O)$ tape recorder signal, the zonal and seasonal means, averaged over the 21 years of the EMAC simulation during JJA (June, July, August) between 10 and 30 km are presented in Fig. 6. In the Supplement, this illustration is also presented for the other seasons (DJF – December, January, February; SON – September, October, November; MAM – March, April, May).

High $\delta D(H_2O)$ values can be seen in the troposphere and in the high latitudes of the upper stratosphere. The minimum in $\delta D(H_2O)$ can be found around the tropical tropopause. This minimum spreads out to the poles at around 15 km and to the upper tropical stratosphere. In the Northern Hemisphere an elevated signal of high tropospheric isotope ratios can be observed around 40° N. At the edge of the tropical tropopause layer, this isotopically enriched water vapour penetrates into the stratosphere along the isentropes, through the tropopause, into the tropical pipe. In the tropics the maximum of this signal is transported upwards across the isentropes. It can still be seen during SON, but hardly during DJF (see Supplement). An elevation of enhanced $\delta D(H_2O)$ values during JJA can also be seen in the northern extratropics up to 18 km. These, however, mix in with the depleted stratospheric $\delta D(H_2O)$ values much quicker than in the tropics and are already not visible anymore in SON.

In this illustration, the origin of the enhanced isotope ratios in the tropical lower stratosphere during JJA, can clearly be associated with elevated isotopically enriched water vapour in the northern hemispheric troposphere. A similar elevation of isotopically enriched tropospheric water vapour can also be observed during DJF at around 40° S (see Supplement). In contrast, this signal is at considerably lower altitudes and does not penetrate into the tropical stratosphere.

When entering the lower stratosphere, air experiences rapid horizontal transport between the tropics and the mid-latitudes above the subtropical jets (Rosenlof et al.,

ACPD
14, 29459–29497, 2014

1997). The region between the 380 and the 400 K isentrope is therefore crucial for the properties of stratospheric air. To provide an insight into the horizontal dynamics of this region, the average of $\delta D(H_2O)$ between the 380 and the 400 K isentrope is shown in a latitude-longitude representation during JJA in Fig. 7. Again the other seasons are presented in the Supplement.

In general, the image features a pattern with low $\delta D(H_2O)$ in the tropics and increasing values with higher latitudes. In the Northern Hemisphere, patterns can be observed, which are associated with the Asian Summer Monsoon (ASM), as well as with the North American Monsoon (NAM). High $\delta D(H_2O)$ values can be seen over the entire North American continent. Over southern Asia, in contrast, very low values are dominant. Around this isotopically depleted centre of the ASM anticyclone, the water vapour is isotopically enriched. Over the Western Pacific, the wind vectors indicate a considerable southward component, which drags isotopically enriched air from the extratropics towards the tropics and westwards hereafter. This air originates from the westerly wind regime at around 40° N over the Asian continent, because a high potential vorticity gradient (not shown) north of this region prevents meridional air mass exchange (see e.g. Plumb, 2002). In the Western Pacific region, furthermore, a lowering of the tropopause is evident. This is likely to be the region where water vapour can enter the stratosphere.

In order to identify the origin of the high $\delta D(H_2O)$ values over the Western Pacific, a zonal cross section, averaged from 30 to 40° N is presented in Fig. 8.

Here, the highest tropospheric $\delta D(H_2O)$ values can be found at around 100° E, above the Himalaya mountains. Another, yet weaker, maximum lies at around 100° W, which is the location of the Mexican High Plateau and the NAM. A third, even weaker maximum at 0° E can be associated with the North African Monsoon. The lowest values are accompanied by the highest parts of the tropopause, which lies at around 16 km altitude at 50° E. This is also where the temperatures are lowest (not shown). The tropopause height exhibits two minima, one around 160° W and one around 10° W. In these minima, the highest stratospheric $\delta D(H_2O)$ values are found. The underlying

ACPD
14, 29459–29497, 2014

westerly wind regime (shown in Fig. 7), connected with the tropopause-crossing isentropes in the subtropics, is thus confirming that the enhanced stratospheric isotope ratios during JJA originate from monsoonal (Asian and American) activity. Isentrope-crossing upward motion of the isotopically enriched water vapour in this region can be explained with strong gravity wave activity, taking place within the jetstreak at the forefront of the ASM anticyclone (see e.g., Reid and Gage, 1996).

These high $\delta D(H_2O)$ values are much more pronounced for the ASM and referring to Fig. 7, only the Western Pacific region provides a strong enough southward wind component to transport this isotopically enriched water vapour into the tropics. This suggests, that the NH summer signal of the stratospheric $\delta D(H_2O)$ tape recorder, which propagates upwards over time, is mainly generated by the ASM.

In order to confirm this assumption, Fig. 9 shows the difference in $\delta D(H_2O)$ between the two main Monsoon regions (a subtraction of the average of 140 to 40° W from the average of 80 to 180° E; in other words, the ASM region minus the NAM region). For guidance, the tropopause and the isentropes (averaged globally) are included here as well. Positive values indicate higher $\delta D(H_2O)$ in the Western Pacific, negative values show enhanced $\delta D(H_2O)$ in the American region.

The most dominant feature of the figure is the patch of very high values in the northern TTL, between 12 and 16 km. This indicates that in the model, convective activity is much stronger in the Western Pacific region than in the American region. Another region with high values can be found above the tropical tropopause at around 17 km altitude. This confirms that the Western Pacific region is dominant for the emergence of high $\delta D(H_2O)$ values in the tropical lower stratosphere during JJA. The patch with negative values between 30 and 50° N and 15 and 17 km suggests that the lack of the southward wind component in the American region leaves more isotopically enriched water vapour at the higher altitudes of the American extratropics.

ACPD
14, 29459–29497, 2014

5.2 Correlation analysis with Monsoon systems

In order to corroborate the hypothesis that ASM activity is crucial for the enhanced $\delta D(H_2O)$ of the tropical tape recorder signal in JJA, a correlation analysis was carried out. For that, the anomalies w.r.t. the 21 year average of the $\delta D(H_2O)$ values between the 370 and the 390 K isentropes in the subtropical Western Pacific (15 to 40° N and 120° E to 140° W) region and in the subtropical American and Western Atlantic region (15 to 40° N and 120 to 20° W) were correlated with the anomalies of the tropical $\delta D(H_2O)$ tape recorder signal in the stratosphere for the 21 years of the EMAC simulation. Figure 10 shows the $\delta D(H_2O)$ values averaged between the 370 and the 390 K isentropes and over the 21 years of the model simulation. The described regions are framed. The regions were selected to be north (15° N) of the tape recorder signal and below the altitude of its maximum, in order not to take the starting region of the tape recorder itself into account. A detailed description of the procedure and the applied Pearson's correlation is provided in the Supplement.

The results are shown in Fig. 11. Since the Monsoon signals for the correlation are taken from JJA, the time axes of the figures start in June. The tape recorder values for the correlation for the months of January to May are always taken from the subsequent year of the ASM signal.

The left panel of Fig. 11 shows a tape recorder signal in the correlation coefficients of the ASM with the $\delta D(H_2O)$ tape recorder signal. While in general this correlation shows values between −0.2 and 0.2, a stripe from 18 km in July to 23 km in April exhibits enhanced correlation values. The highest values, which reach a correlation of up to 0.7 can be seen from July to September between 18 and 19 km. In the following months this "correlation tape recorder" signal weakens with ascent over time and fades out in spring. The right panel of Fig. 11 shows the correlation coefficients between the NAM and the $\delta D(H_2O)$ tape recorder. Here, too, a "correlation tape recorder" signal can be detected, however, with slightly lower correlation coefficients, an earlier fade-out and especially, a smaller region of high correlation values during summer in the lower

ACPD
14, 29459–29497, 2014

stratosphere. The spot between 22 and 25 km from July to October, with high correlation values is surprising and thought to be of different nature than the tape recorder signal. The ascent rate of the "correlation tape recorder" matches with the ascent rate of the actual $\delta D(H_2O)$ tape recorder. This correlation analysis confirms the connection between the strength of the Monsoon systems and the stratospheric tape recorder in $\delta D(H_2O)$ and corroborates that the tropical $\delta D(H_2O)$ signature in the stratosphere is closely related to the ASM.

6 The impact of ice lofting on stratospheric $\delta D(H_2O)$

Both the water vapour mixing ratio and $\delta D(H_2O)$ exhibit enhanced values in the lower stratosphere during JJA. The underlying processes for this, however, may differ in some ways for the two quantities. In order to demonstrate this, the water vapour mixing ratios and $\delta D(H_2O)$ in the upper troposphere lower stratosphere region (UTLS) in JJA are shown in Fig. 12.

Differences in the distribution of the enhanced values can be observed when comparing the two panels. In the left panel, enhanced H_2O mixing ratios can be seen within almost the entire TTL, however, decreasing with altitude and towards the southern latitudes. At the northern edge of the TTL, the high H_2O mixing ratios exceed the tropopause and penetrate into the stratosphere. Some water vapour, however, also intrudes into the stratosphere in the central and the southern TTL. Isotopically enriched water vapour (see right panel) exclusively enters the stratosphere at the northern edge of the TTL. $\delta D(H_2O)$ values of around −600 ‰ can be observed, crossing the tropopause and entering the tropical pipe here. In the central and southern parts of the TTL, the water vapour is isotopically strongly depleted, exhibiting values below −700 ‰. Low $\delta D(H_2O)$ values can be observed down to 14 km altitude in the central and southern TTL, while relatively high water vapour mixing ratios reach up to almost 16 km altitude in this region.

ACPD
14, 29459–29497, 2014

In order to elucidate this difference, the relation between the water vapour mixing ratios and $\delta D(H_2O)$ is presented in Fig. 13. The black crosses denote this relation in the NH (10 and 40° N) and the red crosses in the SH (40 and 10° S), both in JJA from 14 to 20 km.

The red crosses can be found in a $\delta D(H_2O)$ range between roughly −720‰ and −640‰ with water vapour mixing ratios of up to 20 µmol mol^{-1}. A slope of increasing $\delta D(H_2O)$ with increasing water vapour mixing ratios is recognisable. The black crosses cover the range of the SH relations as well, but also spread out to larger water vapour mixing ratios and larger $\delta D(H_2O)$ values. Larger water vapour mixing ratios generally feature enhanced $\delta D(H_2O)$ here as well, but for the same H_2O mixing ratios as in the SH, some of the water vapour in the NH is isotopically enriched. This suggests that the processes, which elevate the water vapour in the respective hemispheres, differ. These are connected to convection and its influence on $\delta D(H_2O)$ through phase transitions. In particular, the much discussed influence of convectively lofted ice crystals (see e.g., Khaykin et al., 2009; Steinwagner et al., 2010; Bolot et al., 2013) is considered to be a major driver of these patterns.

The ice water content in the UTLS for JJA is shown in Fig. 14 in order to reveal interhemispheric differences. Additionally, $\delta D(ice)$ (the deuterium isotope ratio of the ice water content) is contoured in the figure and the height of the tropopause is marked. The white regions denote ice water mixing ratios below 0.1 µmol mol^{-1}.

The ice water mixing ratios show two local altitude maxima in this illustration. One in the inner tropics and another one between 30 and 35° N. The latter maximum additionally features high $\delta D(ice)$ at high altitudes up to the tropopause. Ice features δD values of up to −300‰ in this area, while the isotope ratios of water vapour lie around −600‰ here (see Fig. 12). Convectively lofted ice, which resublimates here, is therefore likely to be responsible for the isotopical enrichment of water vapour in this region of the TTL. This water vapour hereafter intrudes into the tropical stratosphere and generates the NH summer $\delta D(H_2O)$ tape recorder signal.

ACPD
14, 29459–29497, 2014

Regarding the analysis of the origin of the $\delta D(H_2O)$ tape recorder signal (Sect. 5), the corresponding region where the ice lofting takes place is crucial. For this, the ice water content (left panel) and δD(ice) (right panel) in JJA at 14 km altitude are shown in Fig. 15. The altitude of 14 km was chosen because, as can be seen in Fig. 14, at this altitude the inner tropical and the northern subtropical altitude maxima of the ice water content are still pronounced. Regions with ice water mixing ratios below 0.1 $\mu mol\,mol^{-1}$ are again shaded white.

The left panel shows several spots of enhanced ice water mixing ratios around the convective zones in the tropics. Especially, high ice water mixing ratios can be seen in Southeast Asia and Middle America, but by far the highest values are found over the Tibetan Plateau. δD(ice) exhibits a rather uniform picture around the tropics, with values mostly between −500 ‰ and −400 ‰. Only one single spot with isotopically enriched ice water above the Tibetan plateau with values above −200 ‰ strikes the eye. This corresponds with the latitude of the altitude maximum in Fig. 14 and leads back to Sect. 5, where the origin of the NH summer signal of the $\delta D(H_2O)$ tape recorder was traced back to the ASM. Convective activity over the Tibetan Plateau and isotopic enrichment of upper tropospheric water vapour through exceptionally strong ice lofting, can therefore be understood as the starting point of the stratospheric $\delta D(H_2O)$ tape recorder in the EMAC simulation.

7 Summary and discussion

As a first application of the new H2OISO submodel within the EMAC model, stratospheric water vapour isotope ratios were investigated. The time series of water vapour in the here applied EMAC simulation reproduces the major variations of the recent decades. The time series of $\delta D(H_2O)$ shows similarities with H_2O, differs however, mainly regarding short term changes. This suggests that the processes controlling these two quantities coincide, but their effect on the respective value is of different strength.

ACPD
14, 29459–29497, 2014

The impact of methane oxidation on the stratospheric $\delta D(H_2O)$ tape recorder signal was tested by comparing the evaluated EMAC simulation with an additional simulation, with a suppressed chemical effect on $\delta D(H_2O)$. The chemistry mainly affects water vapour and its isotopic signature above 25 km, where the $\delta D(H_2O)$ tape recorder signal fades out faster through this chemical effect. Additionally, the amplitude of the $\delta D(H_2O)$ tape recorder is reduced because methane oxidation influences the low $\delta D(H_2O)$ values and the low water vapour mixing ratios stronger than the higher ones. This result is not surprising, however, it reveals the impact of the isotope chemistry on the tape recorder. Randel et al. (2012) also applied a correction for the methane effect on $\delta D(H_2O)$ to the ACE-FTS satellite retrieval. This lead to the removal of the increase in $\delta D(H_2O)$ with altitude in the stratosphere as well. Moreover, it generated enhanced isotope ratios in the lower stratosphere during JJA and SON, compared to without the methane correction. However, the $\delta D(H_2O)$ tape recorder is still not clearly visible in the satellite retrieval.

The signal of enhanced $\delta D(H_2O)$ during JJA in the lower stratosphere was traced back to its originating region and its determining process in the EMAC simulation. The main origin of the isotopically enriched water vapour during JJA in the lower stratosphere could be associated with the ASM. This water vapour originates from the Tibetan Plateau, crosses the tropopause over the Western Pacific and there, experiences southward transport at the forefront of the ASM anticyclone. The analysis of the correlation coefficient between the anomalies of the $\delta D(H_2O)$ values in the Monsoon regions and the tape recorder signal in $\delta D(H_2O)$ corroborated this connection. Furthermore, it supports the assumption, that the effect of the NAM on the tape recorder is smaller compared to the effect of the ASM. A link between the ASM and the tropical tape recorder in water vapour has already been found by Dethof et al. (1999). The southern flank of the anticyclone moistens the UTLS during JJA and contributes significantly to the stratospheric water vapour budget (see also Bannister et al., 2004; Gettelman and Kinnison, 2004; Lelieveld et al., 2007; James et al., 2008). Also according to Fueglistaler et al. (2004) this side-ways transport into the tropics from the ASM

ACPD
14, 29459–29497, 2014

complements the transport through the tropopause throughout the year. However, for the $\delta D(H_2O)$ tape recorder, Steinwagner et al. (2010) suggest slow dehydration by cirrus clouds to have a key role by analysing MIPAS satellite data. The relative importance of the individual processes for the annual signal have thus to be further investigated.

Augmented convective ice lofting during the ASM season over the Himalaya mountains has been shown to isotopically enrich the water vapour in the upper troposphere. Lateron, this enriched water vapour contributes significantly to the $\delta D(H_2O)$ tape recorder in the EMAC simulation. However, Randel et al. (2012) present a different behaviour of $\delta D(H_2O)$ in the UTLS by analysing ACE-FTS satellite data. In this retrieval, enriched $\delta D(H_2O)$ at 16.5 km altitude can be found only over America and the patch of high $\delta D(H_2O)$ associated with the ASM, as seen in the EMAC data is entirely lacking. Convective ice overshooting is under discussion as to whether having a significant effect on the stratospheric water vapour budget (see i.e. Khaykin et al., 2009). According to Dessler et al. (2007) and Bolot et al. (2013), however, it has a substantial effect on the $\delta D(H_2O)$ signature in the UTLS. This ice overshooting effect performs mostly in the inner tropics and has the potential to isotopically enrich the tropical lower stratosphere. The NAM is also associated with strong convective ice overshooting (Uma et al., 2014). The direct intrusion of ice crystals into the stratosphere, though, is known to be represented rather sparsely by the here applied convection scheme from Tiedtke (1989). Hence, this discrepancy between model and observations may be due to the underrepresentation of convective ice overshooting in the applied convection scheme. The outstanding high isotopic signature in ice over Asia, may hence be an artefact of the underrepresented ice overshooting. The NAM region as well as the inner tropics may posses comparably high $\delta D(ice)$ values in the UTLS. The estimate of the effect of the ASM region on stratospheric $\delta D(H_2O)$ may therefore be distorted. Moreover, this is most likely also the cause for the too low $\delta D(H_2O)$ values in the lower tropical stratosphere in EMAC compared to satellite observations during NH summer, as shown in the companion part 1 of this article (Eichinger et al., 2014). A more detailed evaluation of this effect can be conducted through the implementation and application

ACPD
14, 29459–29497, 2014

of water isotopologues in other convection schemes of EMAC. Future sensitivity studies can then also resolve the robustness of the here discovered patterns and possibly explain the differences between model results and observations more precisely.

8 Conclusions

The temporal variations of stratospheric $\delta D(H_2O)$ reveal connections to those of water vapour. However, the changes show a different behaviour concerning the amplitudes. This provides additional information about the underlying processes of the changes and therefore can help to gain a better understanding of the reasons for the trends and variations of the stratospheric water vapour budget. Beforehand, this requires an understanding and quantification of the influence of the individual processes that are responsible for the patterns of $\delta D(H_2O)$ in the stratosphere.

The isotope effects during methane oxidation blur the $\delta D(H_2O)$ tape recorder signal, by damping its amplitude and overshadowing it at higher altitudes. This explains the weaker tape recorder signal in $\delta D(H_2O)$ compared to those in H_2O and HDO. The origin of enhanced $\delta D(H_2O)$ in the lower stratosphere during NH summer in the EMAC model simulation was traced back to the Asian Summer Monsoon (ASM). Here, strong convection over the Tibetan Plateau lofts ice crystals into the upper troposphere, where these, when resublimating, isotopically enrich the water vapour. This water vapour crosses the tropopause over the Western Pacific and furthermore, follows the monsoonal anticyclone into the tropics. This process was shown to significantly contribute to the $\delta D(H_2O)$ tape recorder signal in the EMAC simulation. However, discrepancies between the model results and satellite retrievals indicate insufficiencies in the model, i.e. the underrepresentation of overshooting convection.

This study has set the basis for further analyses in order to determine the connection between the patterns and changes in stratospheric H_2O and $\delta D(H_2O)$. The additional information provided by the water isotope ratio can be of significant support to unravel

ACPD
14, 29459–29497, 2014

the factors, which contribute to trends and variations in the stratospheric water vapour budget.

The Supplement related to this article is available online at doi:10.5194/acpd-14-29459-2014-supplement.

Acknowledgements. The authors thank the DFG (Deutsche Forschungsgemeinschaft) for funding the research group SHARP (Stratospheric Change and its Role for Climate Prediction, DFG Research Unit 1095); the presented study was conducted as part of R. Eichingers Ph.D. thesis under grant number BR 1559/5-1. We acknowledge support from the Leibnitz Supercomputing Center (LRZ), the German Climate Computing Center (DKRZ) and thank all MESSy developers and submodel maintainers for their support. Moreover, we thank H. Garny for an important impulse and S. Brinkop for important comments on the manuscript.

The service charges for this open access publication have been covered by a Research Centre of the Helmholtz Association.

References

Bannister, R. N., O'Neill, A., Gregory, A. R., and Nissen, K. M.: The role of the south-east Asian monsoon and other seasonal features in creating the 'tape-recorder' signal in the Unified Model, Q. J. Roy. Meteor. Soc., 130, 1531–1554, 2004. 29475

Bolot, M., Legras, B., and Moyer, E. J.: Modelling and interpreting the isotopic composition of water vapour in convective updrafts, Atmos. Chem. Phys., 13, 7903–7935, doi:10.5194/acp-13-7903-2013, 2013. 29461, 29473, 29476

Dee, D. P., Uppala, S. M., Simmons, A. J., Berrisford, P., Poli, P., Kobayashi, S., Andrae, U., Balmaseda, M. A., Balsamo, G., Bauer, P., Bechtold, P., Beljaars, A. C. M., van de Berg, L., Bidlot, J., Bormann, N. B., Delsol, C., Dragani, R., Fuentes, M., Geer, A. J., Haimberger, L., Healy, S. B., Hersbach, H., Hólm, E. V., Isaksen, L., Kållberg, P., Köhler, M., Matricardi, M.,

McNally, A. P., Monge-Sanz, B. M., Morcrette, J.-J., Park, B.-K., Peubey, C., de Rosnay, P., Tavolato, C., Thépaut, J.-N., and Vitart, F.: The ERA-Interim reanalysis: configuration and performance of the data assimilation system, Q. J. Roy. Meteor. Soc., 656, 553–597, 2011. 29463

Dessler, A. E. and Sherwood, S. C.: A model of HDO in the tropical tropopause layer, Atmos. Chem. Phys., 3, 2173–2181, doi:10.5194/acp-3-2173-2003, 2003. 29461

Dessler, A. E., Hanisco, T. F., and Füglistaler, S.: Effects of convective ice lofting on H_2O and HDO in the tropical tropopause layer, J. Geophys. Res.-Atmos., 112, D18309, doi:10.1029/2007JD008609, 2007. 29476

Dessler, A. E., Schoeberl, M. R., Wang, T., Davis, S. M., and Rosenlof, K. H.: Stratospheric water vapor feedback, P. Natl. Acad. Sci. USA, 110, 18087–18091, 2013. 29464

Dethof, A., O'Neill, A., Slingo, J. M., and Smit, H. G. J.: A mechanism for moistening the lower stratosphere involving the Asian summer monsoon, Q. J. Roy. Meteor. Soc., 125, 1079–1106, 1999. 29475

Eichinger, R., Jöckel, P., Brinkop, S., Werner, M., and Lossow, S.: Simulation of the isotopic composition of stratospheric water vapour – Part 1: Description and evaluation of the EMAC model, Atmos. Chem. Phys. Discuss., 14, 23807–23846, doi:10.5194/acpd-14-23807-2014, 2014. 29461, 29463, 29476

Forster, P. M. D. F. and Shine, K. P.: Stratospheric water vapour changes as a possible contributor to observed stratospheric cooling, J. Geophys. Res., 26, 3309–3312, 1999. 29460

Fueglistaler, S., Wernli, H., and Peter, T.: Tropical troposphere-to-stratosphere transport inferred from trajectory calculations, J. Geophys. Res., 109, D03108, doi:, 2004. 29475

Fueglistaler, S., Dessler, A. E., Dunkerton, J. T., Folkins, I., Fu, Q., and Mote, P. W.: Tropical tropopause layer, Rev. Geophys., 47, RG1004, doi:, 2009. 29460

Gettelman, A. and Kinnison, D. E.: Impact of monsoon circulations on the upper troposphere and lower stratosphere, J. Geophys. Res., 109, D22101, doi:, 2004. 29475

Hagemann, R., Nief, G., and Roth, E.: Absolute isotopic scale for deuterium analysis of natural waters. Absolute D/H ratio for SMOW, Tellus, 22, 712–715, 1970. 29462

Hoffmann, G., Werner, M., and Heimann, M.: Water isotope module of the ECHAM atmospheric general circulation model: A study on timescales from days to several years, J. Geophys. Res., 103, 16871–16896, 1998. 29461, 29463

ACPD
14, 29459–29497, 2014

Hurst, D. F., Oltmans, S. J., Vömel, H., Rosenlof, K. H., Davis, S. M., Ray, E. A., Hall, E. G., and Jordan, A. F.: Stratospheric water vapor trends over Boulder, Colorado: analysis of the 30 year Boulder record, J. Geophys. Res., 116, D02306, doi:, 2011. 29464

James, R., Bonazzola, M., Legras, B., Surbled, K., and Fueglistaler, S.: Water vapor transport and dehydration above convective outflow during Asian monsoon, Geophys. Res. Lett., 35, L20810, doi:, 2008. 29475

Jöckel, P., Sander, R., Kerkweg, A., Tost, H., and Lelieveld, J.: Technical Note: The Modular Earth Submodel System (MESSy) – a new approach towards Earth System Modeling, Atmos. Chem. Phys., 5, 433–444, doi:10.5194/acp-5-433-2005, 2005. 29463

Jöckel, P., Kerkweg, A., Buchholz-Dietsch, J., Tost, H., Sander, R., and Pozzer, A.: Technical Note: Coupling of chemical processes with the Modular Earth Submodel System (MESSy) submodel TRACER, Atmos. Chem. Phys., 8, 1677–1687, doi:10.5194/acp-8-1677-2008, 2008. 29463

Jöckel, P., Kerkweg, A., Pozzer, A., Sander, R., Tost, H., Riede, H., Baumgaertner, A., Gromov, S., and Kern, B.: Development cycle 2 of the Modular Earth Submodel System (MESSy2), Geosci. Model Dev., 3, 717–752, doi:10.5194/gmd-3-717-2010, 2010. 29461, 29463

Johnson, D. G., Jucks, K. W., Traub, W. A., and Chance, K. V.: Isotopic composition of stratospheric water vapor: implications for transport, J. Geophys. Res., 106, 12219–12226, 2001. 29461

Khaykin, S., Pommereau, J.-P., Korshunov, L., Yushkov, V., Nielsen, J., Larsen, N., Christensen, T., Garnier, A., Lukyanov, A., and Williams, E.: Hydration of the lower stratosphere by ice crystal geysers over land convective systems, Atmos. Chem. Phys., 9, 2275–2287, doi:10.5194/acp-9-2275-2009, 2009. 29473, 29476

Lelieveld, J., Brühl, C., Jöckel, P., Steil, B., Crutzen, P. J., Fischer, H., Giorgetta, M. A., Hoor, P., Lawrence, M. G., Sausen, R., and Tost, H.: Stratospheric dryness: model simulations and satellite observations, Atmos. Chem. Phys., 7, 1313–1332, doi:10.5194/acp-7-1313-2007, 2007. 29475

Moyer, E. M., Irion, F. W., Yung, Y. L., and Gunson, M. R.: ATMOS stratospheric deuterated water and implications for troposphere-stratosphere transport, Geophys. Res. Lett., 23, 2385–2388, 1996. 29461

Niwano, M., Yamazaki, K., and Shiotani, M.: Seasonal and QBO variations of ascent rate in the tropical lower stratosphere as inferred from UARS HALOE trace gas data, J. Geophys. Res., 108, 4794, doi:, 2003. 29467

ACPD
14, 29459–29497, 2014

Nordeng, T. E.: Extended version of the convection parameterization scheme at ECMWF and their impacts upon the mean climate and transient activity of the model in the tropics, Res. Dep. Tech Memo, 206, 41 pp., Eur. Cent. for Medium-Range Weather Forecast, Reading, Berkshire, UK, 1994. 29463

Plumb, A. R.: Stratospheric transport, J. Meteorol. Soc. Jpn., 80, 793–809, 2002. 29469

Randel, W. J. and Jensen, E. J.: Physical processes in the tropical tropopause layer and their roles in a changing climate, Nat. Geosci., 6, 169–176, 2013. 29464

Randel, W. J., Moyer, E., Park, M., Jensen, E., Bernath, P., Walker, K., and Boone, C.: Global variations of HDO and HDO/H_2O ratios in the upper troposphere and lower stratosphere derived from ACE-FTS satellite measurments, J. Geophys. Res., 117, doi:, 2012. 29462, 29475, 29476

Reid, G. C. and Gage, K. S.: The tropical tropopause over the western Pacific: wave driving, convection, and the annual cycle, J. Geophys. Res., 101, 21233–21241, 1996. 29470

Ridal, M. and Siskind, D. E.: A two-dimensional suimulation of the isotopic composition of water vapor and methane in the upper atmosphere, J. Geophys. Res., 107, D244807, doi:, 2002. 29461

Ridal, M., Jonsson, A., Werner, M., and Murtagh, D. P.: A one-dimensional simulation of the water vapor isotope HDO in the tropical stratosphere, J. Geophys. Res., 106, 32283–32294, 2001. 29461

Rosenlof, K. H., Tuck, A. F., Kelly, K. K., Russel, J. M., and McCormick, M. P.: Hemispheric asymmetries in water vapor and inferences about transport in the lower stratosphere, J. Geophys. Res., 102, 13213–13234, 1997. 29468

Schmidt, G. A., Hoffmann, G., Shindell, D. T., and Hu, Y.: Modeling atmospheric stable water isotopes and the potential for constraining cloud processes and stratosphere–troposphere water exchange, J. Geophys. Res., 110, D21314, doi:, 2005. 29461

Shindell, D. T.: Climate and ozone response to increased stratospheric water vapor, Geophys. Res. Lett., 28, 1551–1554, 2001. 29460

Steinwagner, J., Füglistaler, S., Stiller, G., von Clarmann, T., Kiefer, M., Borsboom, P.-P., van Delden, A., and Röckmann, T.: Tropical dehydration processes constrained by the seasonality of stratospheric deuterated water, Nat. Geosci., 3, 262–266, doi:10.1038/NGEO822, 2010. 29461, 29462, 29473, 29476

Tiedtke, M.: A comprehensive mass flux scheme for cumulus parameterization in large-scale models, Mon. Weather Rev., 117, 1779–1800, 1989. 29463, 29476

ACPD
14, 29459–29497, 2014

Uma, K. N., Das, S. K., and Das, S. S.: A climatological perspective of water vapor at the UTLS region over different global monsoon regions: observations inferred from the Aura-MLS and reanalysis data, Clim. Dynam., 42, 10.1007, 2014. 29476

Werner, M., Heimann, M., and Hoffmann, G.: Isotopic composition and origin of polar precipitation in present and glacial climate simulations, Tellus B, 53B, 53–71, 2001. 29463

Werner, M., Langebroek, P. M., Carlsen, T., Herold, M., and Lohmann, G.: Stable water isotopes in the ECHAM5 general circulation model: toward high-resolution isotope modeling on a global scale, J. Geophys. Res., 116, D15109, doi:, 2011. 29461, 29463

Zahn, A., Franz, P., Bechtel, C., Grooß, J.-U., and Röckmann, T.: Modelling the budget of middle atmospheric water vapour isotopes, Atmos. Chem. Phys., 6, 2073–2090, doi:10.5194/acp-6-2073-2006, 2006. 29461

ACPD
14, 29459–29497, 2014

Simulation of the isotopic composition of stratospheric water vapour – Part 2

R. Eichinger et al.

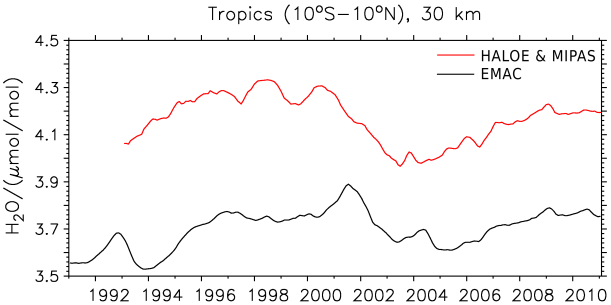

Figure 1. Time series of stratospheric water vapour at 30 km averaged between 10° S and 10° N. Combined HALOE and MIPAS data and the EMAC simulation. Both time series are processed with a two year running mean.

ACPD
14, 29459–29497, 2014

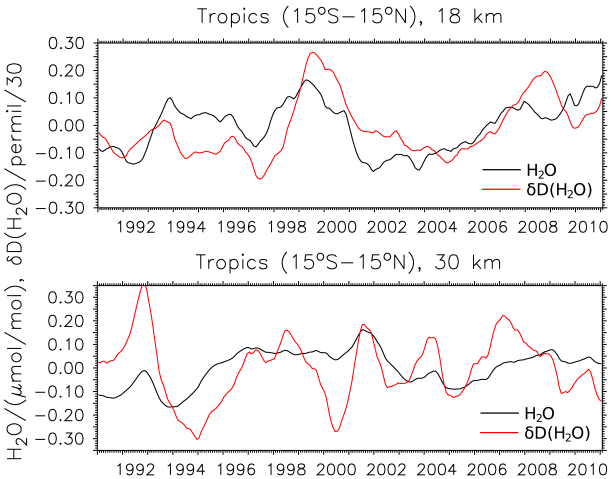

Figure 2. Time series of EMAC simulated monthly stratospheric water vapour (black) and $\delta D(H_2O)$ (red) anomalies w.r.t. the 21 year monthly average at 18 km and at 30 km altitude, averaged between 10° S and 10° N and processed with a two year running mean filter. The $\delta D(H_2O)$ anomalies were scaled with the factor 1/30 for better comparability.

ACPD
14, 29459–29497, 2014

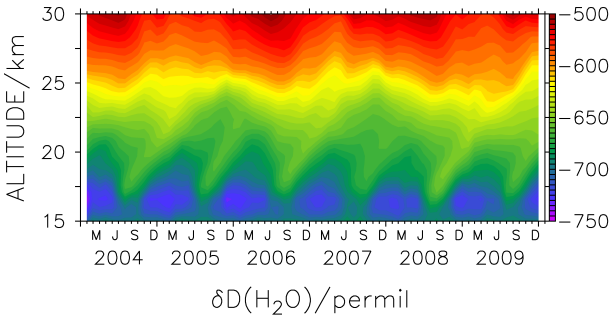

Figure 3. Tropical (15° S–15° N) $\delta D(H_2O)$ tape recorder signal from 2004 to 2009 in the simulation including the effect of methane oxidation on $\delta D(H_2O)$.

ACPD
14, 29459–29497, 2014

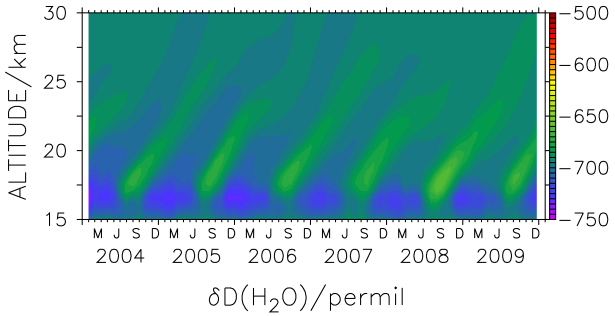

Figure 4. Tropical (15° S–15° N) $\delta D(H_2O)$ tape recorder signal from 2004 to 2009 in the simulation without the effect of methane oxidation on $\delta D(H_2O)$.

ACPD
14, 29459–29497, 2014

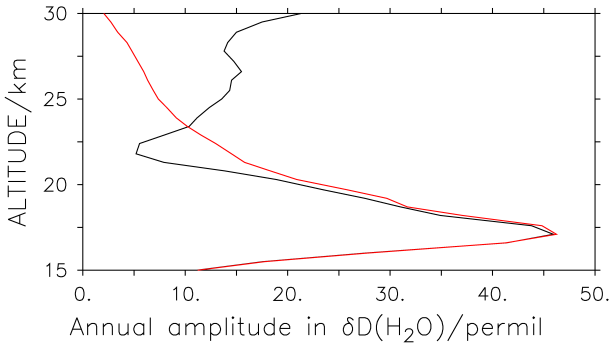

Figure 5. Averaged annual amplitudes of $\delta D(H_2O)$ with altitude, with (black) and without (red) the effect of methane oxidation on $\delta D(H_2O)$.

ACPD
14, 29459–29497, 2014

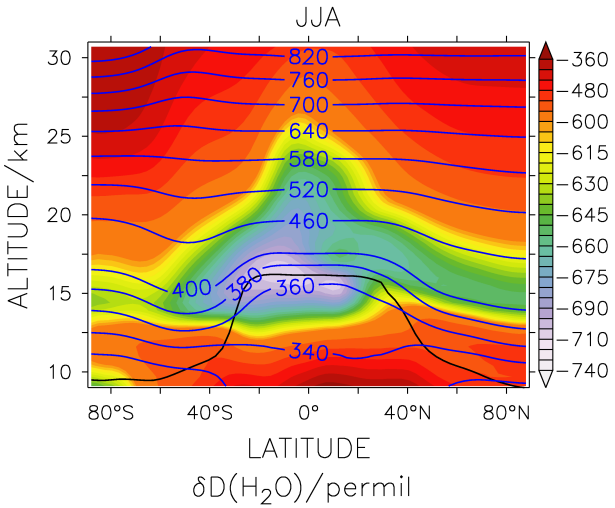

Figure 6. Zonally and seasonally averaged $\delta D(H_2O)$ (coloured), tropopause height (black line) and isentropes (blue contour lines) in K for JJA, averaged over the 21 years of the EMAC simulation.

ACPD
14, 29459–29497, 2014

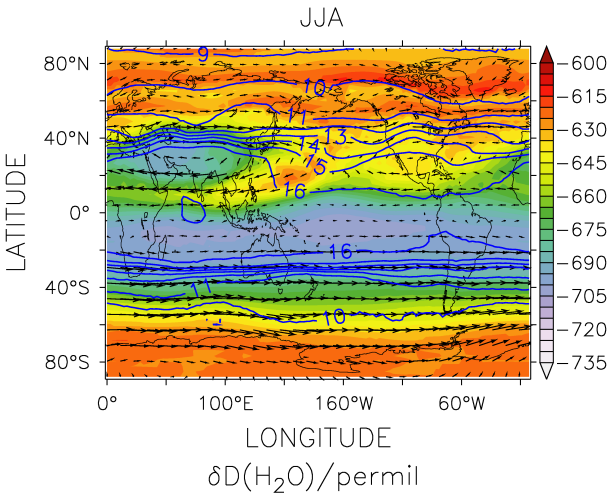

Figure 7. Seasonally averaged $\delta D(H_2O)$ (colours), horizontal wind vectors (arrows) averaged from the 380 to the 400 K isentrope and the tropopause height (blue contour lines) in JJA, averaged over the 21 years of the EMAC simulation.

ACPD
14, 29459–29497, 2014

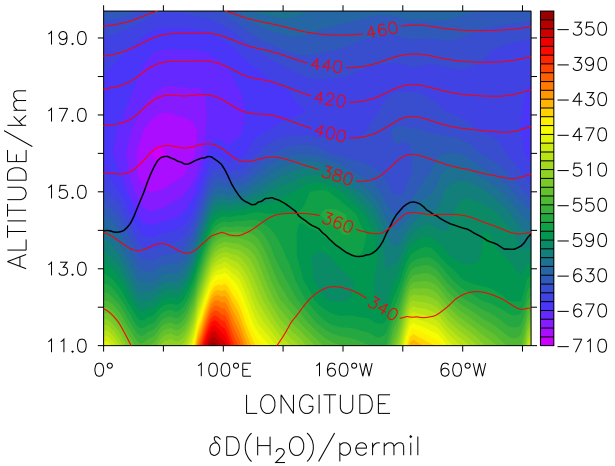

Figure 8. Zonal cross section of $\delta D(H_2O)$, averaged from 30 to 40° N for JJA (averaged over the 21 years of the EMAC simulation). The black line denotes the tropopause height, the red contour lines indicate isentropes (in K).

ACPD
14, 29459–29497, 2014

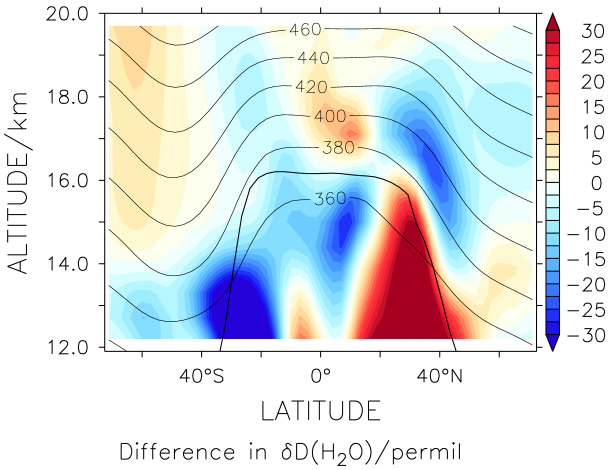

Figure 9. Difference in $\delta D(H_2O)$ between the zonal average from 80 to 180° E and from 140 to 40° W for JJA (ASM minus NAM). The thick line shows the zonally averaged tropopause and the thin contour lines denote the isentropes (both globally averaged).

ACPD
14, 29459–29497, 2014

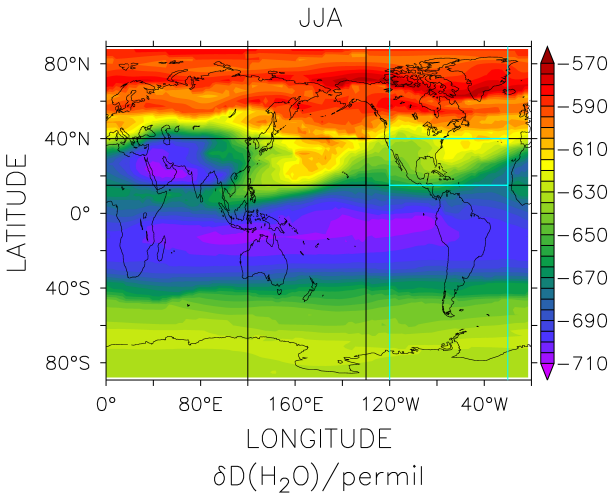

Figure 10. $\delta D(H_2O)$ between the 370 and the 390 K isentrope for JJA, averaged over the 21 years of the EMAC simulation. The frames mark the applied regions (black: ASM, blue: NAM) for the correlation analysis with the tape recorder signal.

ACPD
14, 29459–29497, 2014

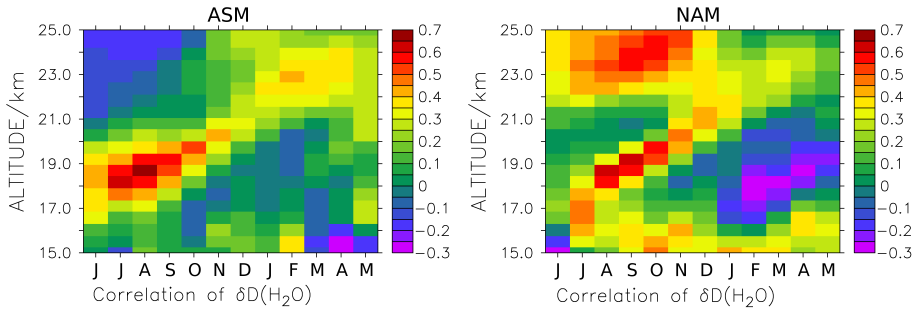

Figure 11. Pearson's correlation coefficient between the $\delta D(H_2O)$ tropical tape recorder signal and the $\delta D(H_2O)$ ASM (left) and NAM (right) signal between the 370 and the 390 K isentrope for the 21 years of the EMAC simulation.

ACPD
14, 29459–29497, 2014

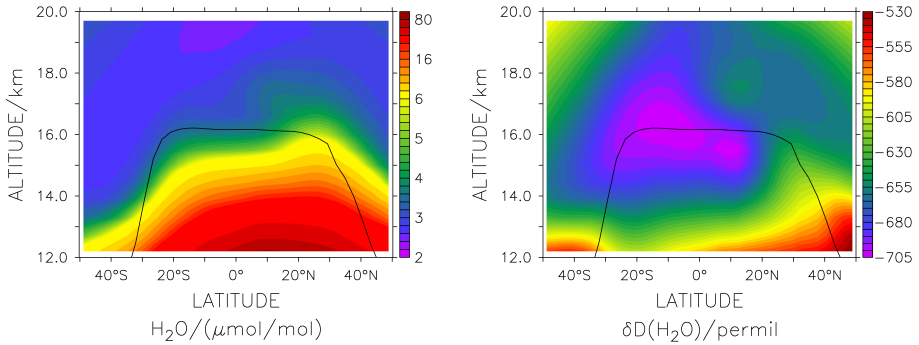

Figure 12. H_2O mixing ratio (left panel) and $\delta D(H_2O)$ (right panel) in the UTLS in JJA and tropopause height (black line), averaged over the 21 years of the EMAC simulation.

ACPD
14, 29459–29497, 2014

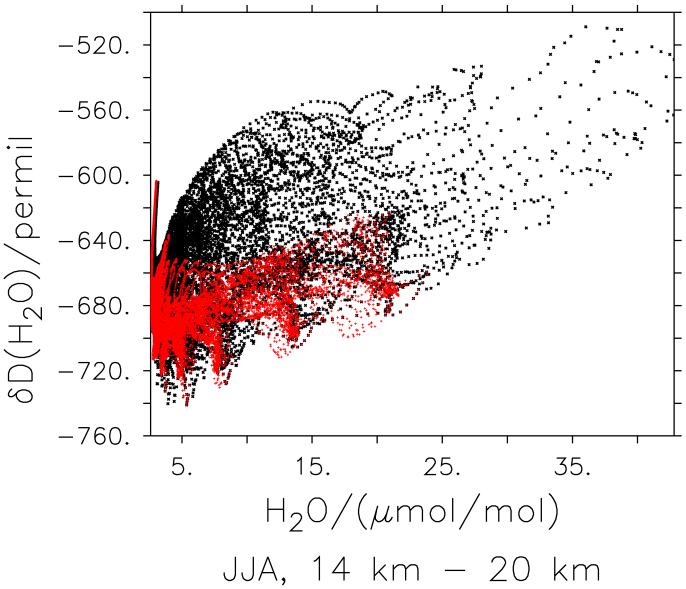

Figure 13. Relation between H_2O and $\delta D(H_2O)$ from 14 to 20 km in JJA between 10 and 40° N (black crosses) and between 40 and 10° S (red crosses), averaged over the 21 years of the EMAC simulation.

ACPD
14, 29459–29497, 2014

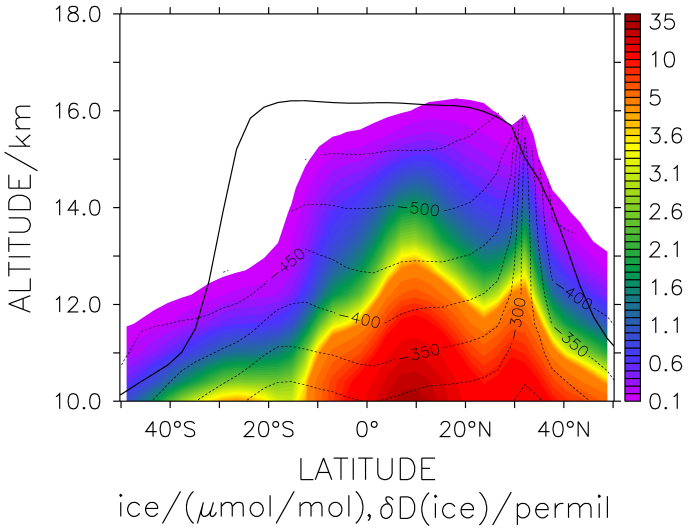

Figure 14. Ice water content (colours) and $\delta D(H_2O)$ in ice (dashed contour lines) in the UTLS in JJA and tropopause height (solid black line), averaged over the 21 years of the EMAC simulation.

ACPD
14, 29459–29497, 2014

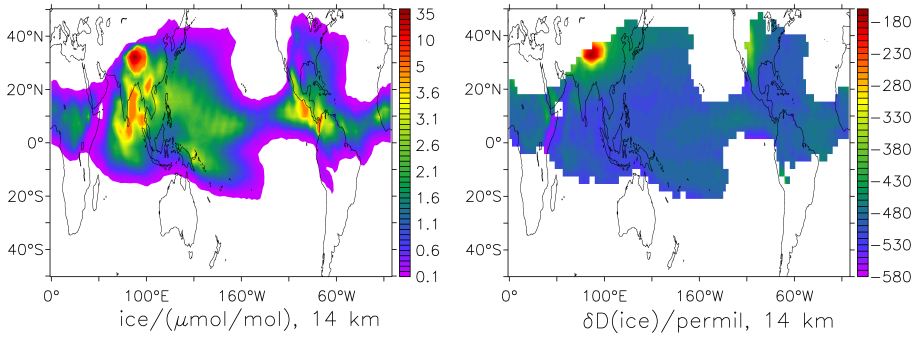

Figure 15. Ice water content (left) and δD(ice) (right) at 14 km altitude in JJA, averaged over the 21 years of the EMAC simulation.

ACPD
14, 29459–29497, 2014